New Journal of Physics
The open access journal at the forefront of physics

Deutsche Physikalische Gesellschaft DPG IOP Institute of Physics

PAPER • OPEN ACCESS

Spatial distributions of the fields in guided normal modes of two coupled parallel optical nanofibers

To cite this article: Fam Le Kien *et al* 2021 *New J. Phys.* **23** 043006

New Journal of Physics
The open access journal at the forefront of physics

Deutsche Physikalische Gesellschaft DPG
IOP Institute of Physics

Published in partnership with: Deutsche Physikalische Gesellschaft and the Institute of Physics

OPEN ACCESS

RECEIVED
10 December 2020

REVISED
15 February 2021

ACCEPTED FOR PUBLICATION
26 February 2021

PUBLISHED
2 April 2021

PAPER

Spatial distributions of the fields in guided normal modes of two coupled parallel optical nanofibers

Fam Le Kien*, Lewis Ruks, Síle Nic Chormaic and Thomas Busch

Okinawa Institute of Science and Technology Graduate University, Onna, Okinawa 904-0495, Japan
* Author to whom any correspondence should be addressed.

E-mail: kienle.pham@oist.jp

Keywords: guided normal modes, coupled nanofibers, field distributions

Abstract

We study the cross-sectional profiles and spatial distributions of the fields in guided normal modes of two coupled parallel optical nanofibers. We show that the distributions of the components of the field in a guided normal mode of two identical nanofibers are either symmetric or antisymmetric with respect to the radial principal axis and the tangential principal axis in the cross-sectional plane of the fibers. The symmetry of the magnetic field components with respect to the principal axes is opposite to that of the electric field components. We show that, in the case of even $\mathcal{E}_z$-cosine modes, the electric intensity distribution is dominant in the area between the fibers, with a saddle point at the two-fiber center. Meanwhile, in the case of odd $\mathcal{E}_z$-sine modes, the electric intensity distribution at the two-fiber center attains a local minimum of exactly zero. We find that the differences between the results of the coupled mode theory and the exact mode theory are large when the separation distance between the fibers is small and either the fiber radius is small or the wavelength of light is large. We show that a slight difference between the radii of the nanofibers leads to strong asymmetry of the intensity distributions of the guided normal modes.

1. Introduction

Coupled waveguides form the central working component in numerous optical devices such as multicore fibers, optical directional couplers, polarization splitters, ring resonators, and interferometers [1–3]. Most of the previous work on coupling between parallel fibers was devoted to conventional fibers where the refractive indices of the core and the cladding differ only slightly from each other and the fiber radius is large compared to the wavelength of light [1–3]. It is desirable to study the properties of guided light fields in coupled subwavelength-diameter optical fibers due to their increasing relevance in current research efforts [4].

Optical nanofibers are tapered fibers that have a subwavelength diameter and significantly differing core and cladding refractive indices [4]. Such ultrathin fibers allow for a guided light field, which is tightly confined radially, to propagate along the fiber for a long distance (with several millimeters being typical) and to interact efficiently with nearby quantum or classical emitters, absorbers, and scatterers [5–7]. Optical nanofibers have been investigated for use in a variety of applications in nonlinear optics, atomic physics, quantum optics, and nanophotonics [4–7]. Nanofibers have been used for atom trapping [8–11], efficient channeling of emission from atoms into fiber-guided modes [12–14], efficient absorption of guided light by atoms [15, 16], generation of Rydberg states of atoms [17], and excitation of quadrupole transitions of atoms [18, 19]. Additionally, slot nanofibers, where the center of the nanofiber has been removed to create two parallel waveguide channels, have been proposed as atom traps [20]. Trapping atoms between two parallel nanofibers and interfacing them with the guided fields of the two different nanofibers may open up more possibilities for applications in nonlinear optics, quantum optics, and quantum information.

Recently, miniaturized optical devices comprising of twisted or knotted nanofibers have been produced [21]. Coupling between two nanofibers in such systems has been studied by using the linear coupling theory

[21, 22], which is an approximate theory valid under the condition of weak coupling [1–3]. It has been shown that butt coupling and self coupling [1–3] could be quite substantial for nanofibers due to the significant mode spread and overlap [22]. In the case of strong coupling between two fibers, a rigorous treatment for the normal modes is required.

The exact guided normal modes of two coupled dielectric rods can be calculated by the expansion of circular harmonics [23]. This method has been extended to the case of multicore fibers [24–26]. A vector theory that uses the circular harmonics expansion method and the finite-element method has been developed for two-core fibers with core index profiles that are radially inhomogeneous [27]. The propagation constant and the flux density of the field in a guided normal mode have been calculated [23, 27, 28]. It has been shown that the coupled mode theory (CMT) performs well when the separation between the fibers is large [23, 27, 28], and gives reasonable results even for touching fibers when the fiber radii are sufficiently large [28]. The polarization patterns [27] and the mode cutoffs [29] have been investigated. In optomechanics, forces arising from internal illumination by light traveling in coupled waveguides have been studied [30], and light-guiding arrays of mechanically compliant glass nanospikes have recently been fabricated [31].

In this work, we investigate the spatial distributions of the fields in guided normal modes of two coupled parallel optical nanofibers. We find that the distributions of the components of the fields in guided normal modes of two coupled identical nanofibers are either symmetric or antisymmetric with respect to the principal axes of the cross-sectional plane of the fibers. We reveal that the intensity distributions of the fields in guided normal modes of two identical fibers attain a local critical point at the two-fiber center that may be used for atom trapping and guiding. Additionally, we show that the discrepancy between the results of the CMT and the exact theory is large when the fiber separation distance is small and either the fiber radius is small or the light wavelength is large.

The key advance of the present work in relation to our previous work [22] is that here we perform an exact treatment for the spatial distributions of the fields in guided normal modes of two nanofibers, while in [22] we used the CMT and calculated the coupling coefficients.

The paper is organized as follows. In section 2 we describe the model of two coupled parallel nanofibers and present the basic equations for guided normal modes. Section 3 contains the numerical calculations of the spatial distributions of the fields in the guided normal modes. Finally, we conclude in section 4.

2. Two coupled parallel optical nanofibers

We study two vacuum-clad, optical nanofibers that are parallel to each other in the direction of the fiber axis z (see figure 1). The fibers are labeled by the indices $j = 1, 2$. Each nanofiber j can be treated as a dielectric cylinder with a radius a_j and a refractive index $n_j > 1$, surrounded by an infinite background of vacuum or air with a refractive index $n_0 = 1$. The nanofiber diameters are a few hundreds of nanometers. An individual nanofiber j can support either a single or multiple modes and this depends on the fiber size parameter $V_j = ka_j\sqrt{n_j^2 - n_0^2}$. Here, $k = \omega/c$ is the wave number of light with optical frequency ω in free space. We neglect the van der Waals interaction between the fibers assuming that they are fixed.

We note that, although the configurations of twisted and knotted nanofibers have been experimentally realized [21], the technique used in that work does not allow one to obtain the configuration of two parallel nanofibers with high quality. Since nanofibers are usually fabricated by tapering of single-mode fibers [4], the large conic transition regions make it very challenging to obtain the configuration of two coupled parallel nanofibers with high quality. Despite this fact, we believe that the model can, in principle, be experimentally realized with a reasonable quality in the future. Alternatively, pulled nanofibers do not have a comparable conical transition region and offer a configuration that could be more easily experimentally realizable [32].

We introduce the global Cartesian coordinate system $\{x, y, z\}$. Here, the z axis is parallel to the z_1 and z_2 axes of the fibers, the x axis is perpendicular to the z axis and connects the centers O_1 and O_2 of the fibers, and the y axis is perpendicular to the x and z axes (see figure 1). The plane xy is the transverse (cross-sectional) plane of the fibers. The x and y axes are called the radial and tangential axes, respectively, of the two-fiber system (see figure 1(b)). The positions of the fiber centers O_1 and O_2 on the x axis are $O_1 = -(a_1 + d_1)$ and $O_2 = a_2 + d_2$, where $d_1 + d_2 = d$ is the fiber separation distance. Without loss of generality, we choose $d_1 = d_2 = d/2$. For each individual fiber j, we use the local fiber-based system $\{r_j, \varphi_j\}$ of polar coordinates.

The normal modes of the coupled fibers are termed array modes. We study the array modes of a light field with an optical frequency ω which propagates in the $+z$ direction with a propagation constant β. The

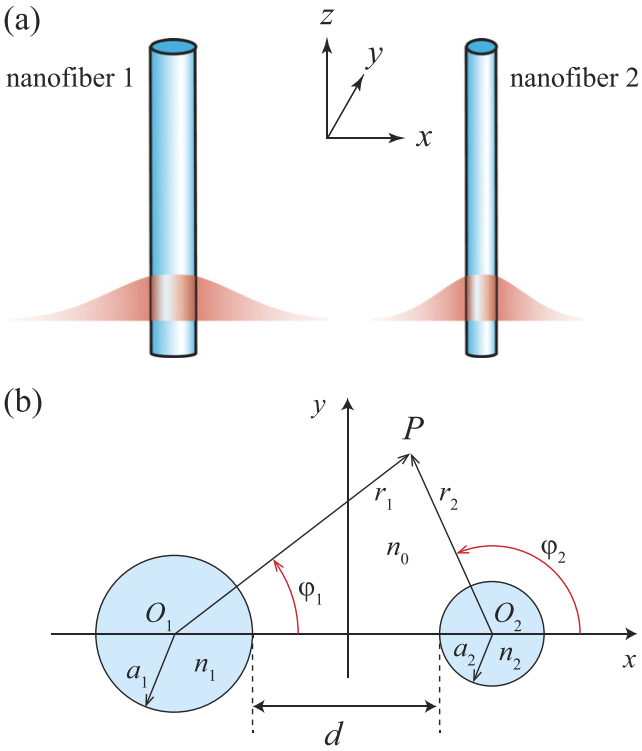

Figure 1. Two coupled parallel optical nanofibers (a) and the geometry of the system (b).

electric and magnetic components of the field can be written as $\mathbf{E} = [\boldsymbol{\mathcal{E}} e^{-i(\omega t-\beta z)} + \text{c.c.}]/2$ and $\mathbf{H} = [\boldsymbol{\mathcal{H}} e^{-i(\omega t-\beta z)t} + \text{c.c.}]/2$, respectively, where $\boldsymbol{\mathcal{E}}$ and $\boldsymbol{\mathcal{H}}$ are the slowly varying complex envelopes.

We are interested in the guided (bound) modes whose fields decay in the transverse direction. The exact theory for the guided normal modes of two parallel dielectric cylinders has been formulated in [23]. The flux density and the beat wavelength for the energy beating between the guided normal modes have been calculated for the cylinders with $a_j \gg \lambda/2$ and $n_j/n_0 \simeq 1$. We follow the theory of [23] and use it to treat the spatial distributions of the fields in the guided normal modes of the coupled nanofibers.

According to the theory of [23], the longitudinal components $\mathcal{E}_z$ and $\mathcal{H}_z$ of the electric and magnetic parts, respectively, of the field in a guided normal mode are given, inside fiber $j = 1, 2$, as

$$\begin{aligned} \mathcal{E}_z &= \sum_{n=0}^{\infty} [A_{nj} J_n(h_j r_j) \cos n\varphi_j + E_{nj} J_n(h_j r_j) \sin n\varphi_j], \\ \mathcal{H}_z &= \sum_{n=0}^{\infty} [B_{nj} J_n(h_j r_j) \sin n\varphi_j + F_{nj} J_n(h_j r_j) \cos n\varphi_j], \end{aligned} \tag{1}$$

and, outside the two fibers, as

$$\begin{aligned} \mathcal{E}_z &= \sum_{j=1}^{2} \sum_{n=0}^{\infty} [C_{nj} K_n(q r_j) \cos n\varphi_j + G_{nj} K_n(q r_j) \sin n\varphi_j], \\ \mathcal{H}_z &= \sum_{j=1}^{2} \sum_{n=0}^{\infty} [D_{nj} K_n(q r_j) \sin n\varphi_j + H_{nj} K_n(q r_j) \cos n\varphi_j]. \end{aligned} \tag{2}$$

Here, we have introduced the fiber parameters

$$h_j = \sqrt{k^2 n_j^2 - \beta^2}, \qquad q = \sqrt{\beta^2 - k^2 n_0^2}, \tag{3}$$

which determine the scales of the spatial variations of the field both inside and outside the fibers. In equations (1) and (2), J_n represents the Bessel functions of the first kind and K_n represents the modified Bessel functions of the second kind. The sets $\{A_{nj}, B_{nj}, C_{nj}, D_{nj}\}$ and $\{E_{nj}, F_{nj}, G_{nj}, H_{nj}\}$ contain the mode expansion coefficients for the $\mathcal{E}_z$-cosine (x-polarized) and $\mathcal{E}_z$-sine (y-polarized) modes, respectively. These coefficients characterize the contributions of the partial waves, associated with the circular harmonics, to

the mode. We emphasize that equations (2) stand for guided (bound) modes but not for radiation (unbound) modes. Therefore, equations (2) do not contain the Hankel functions and the modified Bessel functions of the first kind.

It follows from the Maxwell equations and the translational symmetry of the system in the z direction that the transverse components $\mathcal{E}_{x,y}$ and $\mathcal{H}_{x,y}$ of the electric and magnetic parts of the field can be expressed in terms of the longitudinal components $\mathcal{E}_z$ and $\mathcal{H}_z$ as [1–3]

$$\begin{aligned}
\mathcal{E}_x &= \frac{\mathrm{i}\beta}{k^2 n_{\mathrm{ref}}^2 - \beta^2}\left(\frac{\partial}{\partial x}\mathcal{E}_z + \frac{\omega\mu_0}{\beta}\frac{\partial}{\partial y}\mathcal{H}_z\right),\\
\mathcal{E}_y &= \frac{\mathrm{i}\beta}{k^2 n_{\mathrm{ref}}^2 - \beta^2}\left(\frac{\partial}{\partial y}\mathcal{E}_z - \frac{\omega\mu_0}{\beta}\frac{\partial}{\partial x}\mathcal{H}_z\right),\\
\mathcal{H}_x &= \frac{\mathrm{i}\beta}{k^2 n_{\mathrm{ref}}^2 - \beta^2}\left(\frac{\partial}{\partial x}\mathcal{H}_z - \frac{\omega\epsilon_0 n_{\mathrm{ref}}^2}{\beta}\frac{\partial}{\partial y}\mathcal{E}_z\right),\\
\mathcal{H}_y &= \frac{\mathrm{i}\beta}{k^2 n_{\mathrm{ref}}^2 - \beta^2}\left(\frac{\partial}{\partial y}\mathcal{H}_z + \frac{\omega\epsilon_0 n_{\mathrm{ref}}^2}{\beta}\frac{\partial}{\partial x}\mathcal{E}_z\right).
\end{aligned} \tag{4}$$

Here, n_{ref} is the spatial distribution of the refractive index in the presence of the two-fiber system, that is, $n_{\mathrm{ref}} = n_j$ inside fiber $j = 1, 2$ and $n_{\mathrm{ref}} = n_0$ outside the two fibers.

The field in the mode must satisfy the boundary conditions at the surfaces of both fibers. These conditions say that the tangential components of the electric and magnetic fields are continuous at the boundary. By using the boundary conditions, the algebraic equations for the mode expansion coefficients $\{A_{nj}, B_{nj}, C_{nj}, D_{nj}\}$ and $\{E_{nj}, F_{nj}, G_{nj}, H_{nj}\}$ have been derived [23]. These equations are summarized in appendix A.

For the $\mathcal{E}_z$-cosine modes, the expansion coefficients E_{nj}, F_{nj}, G_{nj}, and H_{nj} vanish. For these modes, the coefficients A_{nj} and B_{nj} for the field inside the fibers are given by equations (A.4), while the coefficients C_{nj} and D_{nj} for the field outside the fibers are nonzero solutions of equations (A.5).

For the $\mathcal{E}_z$-sine modes, the expansion coefficients A_{nj}, B_{nj}, C_{nj}, and D_{nj} vanish. For these modes, the coefficients E_{nj} and F_{nj} for the field inside the fibers are given by equations (A.10), while the coefficients G_{nj} and H_{nj} for the field outside the fibers are nonzero solutions of equations (A.11).

The dispersion equation for the $\mathcal{E}_z$-cosine or $\mathcal{E}_z$-sine modes is $\Delta = 0$, where Δ is the determinant of the system of linear equations (A.5) for C_{nj} and D_{nj} or (A.11) for G_{nj} and H_{nj}. The solution to the equation $\Delta = 0$ determines the propagation constant β, which allows us to calculate the other fiber parameters h_j and q [see equations (3)].

Note that the coefficients associated with C_{nj} and D_{nj} in equations (A.5) and with G_{nj} and H_{nj} in equations (A.11) are real-valued coefficients. Therefore, when we omit a common global phase, we can make $\{A_{nj}, B_{nj}, C_{nj}, D_{nj}\}$ and, similarly, $\{E_{nj}, F_{nj}, G_{nj}, H_{nj}\}$ to be real-valued coefficients. Then, the longitudinal field components $\mathcal{E}_z$ and $\mathcal{H}_z$, given by equations (1) and (2), are real-valued, while the transverse components $(\mathcal{E}_x, \mathcal{E}_y)$ and $(\mathcal{H}_x, \mathcal{H}_y)$, given by equations (4), are imaginary-valued. Thus, we have

$$\begin{aligned}
\mathcal{E}_z^* &= \mathcal{E}_z, \qquad & \mathcal{H}_z^* &= \mathcal{H}_z,\\
\mathcal{E}_x^* &= -\mathcal{E}_x, \qquad & \mathcal{H}_x^* &= -\mathcal{H}_x,\\
\mathcal{E}_y^* &= -\mathcal{E}_y, \qquad & \mathcal{H}_y^* &= -\mathcal{H}_y.
\end{aligned} \tag{5}$$

Equations (5) indicate that the longitudinal components $\mathcal{E}_z$ and $\mathcal{H}_z$ of the field in a guided normal mode are $\pi/2$ out of phase with respect to the transverse components $\mathcal{E}_x$, $\mathcal{E}_y$, $\mathcal{H}_x$, and $\mathcal{H}_y$. This relative phase is a typical feature of guided [1–3] and other transversely confined light fields [33].

Let us consider the particular case where the two fibers are identical, that is, the two fibers have the same radius $a_1 = a_2 = a$ and the same core refractive index $n_1 = n_2 = n_{\mathrm{f}}$. In this case, for the $\mathcal{E}_z$-cosine modes, we find

$$\begin{aligned}
A_{n2} &= (-1)^n \nu A_{n1}, \qquad & B_{n2} &= (-1)^n \nu B_{n1},\\
C_{n2} &= (-1)^n \nu C_{n1}, \qquad & D_{n2} &= (-1)^n \nu D_{n1},
\end{aligned} \tag{6}$$

and, for the $\mathcal{E}_z$-sine modes, we get

$$\begin{aligned}
E_{n2} &= (-1)^n \nu E_{n1}, \qquad & F_{n2} &= (-1)^n \nu F_{n1},\\
G_{n2} &= (-1)^n \nu G_{n1}, \qquad & H_{n2} &= (-1)^n \nu H_{n1},
\end{aligned} \tag{7}$$

Table 1. Symmetry (+) and antisymmetry (−) of the components of the fields in the guided normal modes of two coupled identical fibers with respect to the transformation $x \to -x$.

Mode type	$\mathcal{E}_x$	$\mathcal{E}_y$	$\mathcal{E}_z$	$\mathcal{H}_x$	$\mathcal{H}_y$	$\mathcal{H}_z$
Even $\mathcal{E}_z$-cosine	+	−	−	−	+	+
Odd $\mathcal{E}_z$-cosine	−	+	+	+	−	−
Even $\mathcal{E}_z$-sine	−	+	+	+	−	−
Odd $\mathcal{E}_z$-sine	+	−	−	−	+	+

where $\nu = -1$ or $+1$ corresponds to the even or odd mode, respectively [23]. Then, equations (A.5) for the $\mathcal{E}_z$-cosine modes reduce to equations (A.14) and equations (A.11) for the $\mathcal{E}_z$-sine modes lead to equations (A.15).

After performing the transformation $x \to -x$, that is, $(x, y) \to (-x, y)$, we have $(r_1, \varphi_1) \to (r_2, \pi - \varphi_2)$ and $(r_2, \varphi_2) \to (r_1, \pi - \varphi_1)$. It follows from the relations (6) and (7) and equations (1), (2) and (4) that the field components of the even $\mathcal{E}_z$-cosine and odd $\mathcal{E}_z$-sine modes satisfy the relations [27]

$$\begin{aligned} \mathcal{E}_x(-x,y) &= \mathcal{E}_x(x,y), & \mathcal{H}_x(-x,y) &= -\mathcal{H}_x(x,y), \\ \mathcal{E}_y(-x,y) &= -\mathcal{E}_y(x,y), & \mathcal{H}_y(-x,y) &= \mathcal{H}_y(x,y), \\ \mathcal{E}_z(-x,y) &= -\mathcal{E}_z(x,y), & \mathcal{H}_z(-x,y) &= \mathcal{H}_z(x,y), \end{aligned} \tag{8}$$

and the field components of the odd $\mathcal{E}_z$-cosine and even $\mathcal{E}_z$-sine modes obey the relations [27]

$$\begin{aligned} \mathcal{E}_x(-x,y) &= -\mathcal{E}_x(x,y), & \mathcal{H}_x(-x,y) &= \mathcal{H}_x(x,y), \\ \mathcal{E}_y(-x,y) &= \mathcal{E}_y(x,y), & \mathcal{H}_y(-x,y) &= -\mathcal{H}_y(x,y), \\ \mathcal{E}_z(-x,y) &= \mathcal{E}_z(x,y), & \mathcal{H}_z(-x,y) &= -\mathcal{H}_z(x,y). \end{aligned} \tag{9}$$

The symmetry properties of the components of the fields in the guided normal modes of two coupled identical fibers with respect to the transformation $x \to -x$ are summarized in table 1.

After performing the transformation $y \to -y$, that is, $(x, y) \to (x, -y)$, we have $(r_1, \varphi_1) \to (r_1, -\varphi_1)$ and $(r_2, \varphi_2) \to (r_2, -\varphi_2)$. It follows from equations (1), (2) and (4) that the field components of the $\mathcal{E}_z$-cosine modes satisfy the relations [27]

$$\begin{aligned} \mathcal{E}_x(x,-y) &= \mathcal{E}_x(x,y), & \mathcal{H}_x(x,-y) &= -\mathcal{H}_x(x,y), \\ \mathcal{E}_y(x,-y) &= -\mathcal{E}_y(x,y), & \mathcal{H}_y(x,-y) &= \mathcal{H}_y(x,y), \\ \mathcal{E}_z(x,-y) &= \mathcal{E}_z(x,y), & \mathcal{H}_z(x,-y) &= -\mathcal{H}_z(x,y), \end{aligned} \tag{10}$$

and the field components of the $\mathcal{E}_z$-sine modes obey the relations [27]

$$\begin{aligned} \mathcal{E}_x(x,-y) &= -\mathcal{E}_x(x,y), & \mathcal{H}_x(x,-y) &= \mathcal{H}_x(x,y), \\ \mathcal{E}_y(x,-y) &= \mathcal{E}_y(x,y), & \mathcal{H}_y(x,-y) &= -\mathcal{H}_y(x,y), \\ \mathcal{E}_z(x,-y) &= -\mathcal{E}_z(x,y), & \mathcal{H}_z(x,-y) &= \mathcal{H}_z(x,y). \end{aligned} \tag{11}$$

Note that equations (10) and (11) remain valid for nonidentical fibers. The symmetry properties of the components of the fields in the guided normal modes of two coupled fibers with respect to the transformation $y \to -y$ are summarized in table 2.

Thus, the field components $\mathcal{E}_{x,y,z}$ and $\mathcal{H}_{x,y,z}$ are either symmetric or antisymmetric with respect to the transformations $x \to -x$ and $y \to -y$. This arises because the principal axes x and y are the symmetry axes of the system of two identical fibers. We note that the symmetry of the magnetic field components $\mathcal{H}_{x,y,z}$ with respect to the transformation $x \to -x$ or $y \to -y$ is opposite to that of the electric field components $\mathcal{E}_{x,y,z}$. The symmetry relations (8)–(11) are in agreement with the results of [27].

It is worth noting that, for the odd $\mathcal{E}_z$-sine mode, we have the relations $\mathcal{E}_x(x, y) = -\mathcal{E}_x(x, -y)$, $\mathcal{E}_y(x, y) = -\mathcal{E}_y(-x, y)$, and $\mathcal{E}_z(x, y) = -\mathcal{E}_z(-x, y)$, indicating the antisymmetry of $\mathcal{E}_x$ about the x axis and that of $\mathcal{E}_y$ and $\mathcal{E}_z$ about the y axis. It follows from these relations that, for the odd $\mathcal{E}_z$-sine mode, the electric field $\boldsymbol{\mathcal{E}}$ at the two-fiber center $(x, y) = (0, 0)$ is zero, that is, $\boldsymbol{\mathcal{E}}(0, 0) = 0$.

The vanishing of the electric field $\boldsymbol{\mathcal{E}}$ of the odd $\mathcal{E}_z$-sine mode at the two-fiber center can be used to produce a local minimum of a blue-detuned optical dipole potential to trap ground-state atoms [34–36] or a local minimum of a ponderomotive optical Rydberg-electron potential to trap Rydberg atoms [37, 38].

Table 2. Symmetry (+) and antisymmetry (−) of the components of the fields in the guided normal modes of two coupled fibers with respect to the transformation $y \to -y$.

Mode type	$\mathcal{E}_x$	$\mathcal{E}_y$	$\mathcal{E}_z$	$\mathcal{H}_x$	$\mathcal{H}_y$	$\mathcal{H}_z$
$\mathcal{E}_z$-cosine	+	−	+	−	+	−
$\mathcal{E}_z$-sine	−	+	−	+	−	+

Similarly, we can show that, in the case of the odd $\mathcal{E}_z$-cosine mode, the magnetic field $\boldsymbol{\mathcal{H}}$ at the two-fiber center is zero, that is, $\boldsymbol{\mathcal{H}}(0,0) = 0$.

3. Numerical calculations

In this section, we numerically calculate the propagation constants and spatial distributions of the fields in guided normal modes of two parallel vacuum-clad silica nanofibers. The refractive index of the vacuum cladding is $n_0 = 1$. To calculate the refractive index $n_1 = n_2 = n_f$ of the silica cores of the nanofibers, the four-term Sellmeier formula for fused silica is used [39, 40]. In particular, for light with the wavelength $\lambda = 800$ nm, we have $n_f = 1.4533$. In our numerical calculations, the infinite number of circular harmonics is truncated at a finite number N_{max} in the range from 9 to 19. The value of N_{max} is chosen such that the propagation constant converges and the boundary conditions are satisfied with a reasonable accuracy [23].

According to the previous section, in the case of identical fibers, there are four kinds of normal modes, denoted as even $\mathcal{E}_z$-cosine, odd $\mathcal{E}_z$-cosine, even $\mathcal{E}_z$-sine, and odd $\mathcal{E}_z$-sine modes, or as $I_0^{(\cos)}$, $I_\pi^{(\cos)}$, $I_0^{(\sin)}$, and $I_\pi^{(\sin)}$ modes, respectively [23]. The even $\mathcal{E}_z$-cosine, odd $\mathcal{E}_z$-cosine, even $\mathcal{E}_z$-sine, and odd $\mathcal{E}_z$-sine modes can also be labeled by the letters OO, OE, EE, and EO, respectively. These letters indicate the symmetry (E) and antisymmetry (O) of the field component $\mathcal{E}_y$ about the x (first letter) and y (second letter) axes [27]. We are interested in the case where the fiber radii are small enough that no more than one normal mode of each of the four kinds can be supported.

3.1. Propagation constants of guided normal modes of two identical nanofibers

Let us assume that the two nanofibers have the same fiber radius, that is, $a_1 = a_2 = a$. We plot in figures 2–4 the propagation constant β, normalized to the free-space wave number k, as functions of the fiber radius a, the light wavelength λ, and the fiber separation distance d. We note that the ratio $n_{eff} \equiv \beta/k$ between β and k is called the effective refractive index. It is clear from figures 2–4 that n_{eff} depends on the parameters of the fibers, the wavelength of light, and the mode type. We observe from the figures that there are four guided normal modes, identified as even $\mathcal{E}_z$-cosine, odd $\mathcal{E}_z$-cosine, even $\mathcal{E}_z$-sine, and odd $\mathcal{E}_z$-sine modes [23].

Figures 2–4 show that there are two pairs of adjacent curves. The upper pair corresponds to the even modes and the lower pair to the odd modes. This indicates that the propagation constant of an even mode (see the upper pair of curves) is larger than that of the corresponding odd mode (see the lower pair of curves). The differences between the propagation constants for the odd $\mathcal{E}_z$-cosine and odd $\mathcal{E}_z$-sine modes (see the lower pair of curves) are smaller than those for the even $\mathcal{E}_z$-cosine and even $\mathcal{E}_z$-sine modes (see the upper pair of curves). We see from figure 4 that the differences between the propagation constants for the four guided array modes reduce with increasing fiber separation distance d. We observe from figures 2 and 3 that the odd $\mathcal{E}_z$-cosine and odd $\mathcal{E}_z$-sine modes have cutoffs but the even $\mathcal{E}_z$-cosine and even $\mathcal{E}_z$-sine modes have no cutoff [23, 29]. The reason is the following:

For a single propagation direction $+z$, each single-mode nanofiber can support a superposition of two fundamental modes HE_{11} that are quasilinearly polarized along the x and y axes and are called as $\mathcal{E}_z$-cosine and $\mathcal{E}_z$-sine modes, respectively. We expect that two coupled parallel single-mode nanofibers can support up to four guided normal modes. We introduce the notation $\mathbf{e}_j^{(p)}$ for the profile function of the single-fiber mode with the quasilinear polarization $p = x, y$ of nanofiber $j = 1, 2$. According to the CMT [3], there is no coupling between the principal x and y polarizations. For a suitable choice of the global phases of the mode functions, the approximate profile functions of the guided normal modes can be given as $\mathbf{e}_\pm^{(p)} \simeq \mathbf{e}_1^{(p)} \pm \mathbf{e}_2^{(p)}$, where the sign + and − corresponds to the even and odd modes, respectively. Note that $\mathbf{e}_1^{(p)}(\mathbf{r}) = \mathbf{e}_2^{(p)}(\mathbf{r} + \overrightarrow{O_1O_2})$. When either the fiber radius is small enough or the light wavelength is large enough, we can use the approximation $\mathbf{e}_1^{(p)}(\mathbf{r}) \simeq \mathbf{e}_2^{(p)}(\mathbf{r})$. In these limits, the even array modes with the profile functions $\mathbf{e}_+^{(p)} \simeq \mathbf{e}_1^{(p)} + \mathbf{e}_2^{(p)}$ approach the modes of single nanofibers, while the odd array modes with the profile functions $\mathbf{e}_-^{(p)} \simeq \mathbf{e}_1^{(p)} - \mathbf{e}_2^{(p)}$ are widely spread out in the outside of the nanofibers. Consequently, the propagation constant of an even mode is larger than that of the corresponding odd mode (see

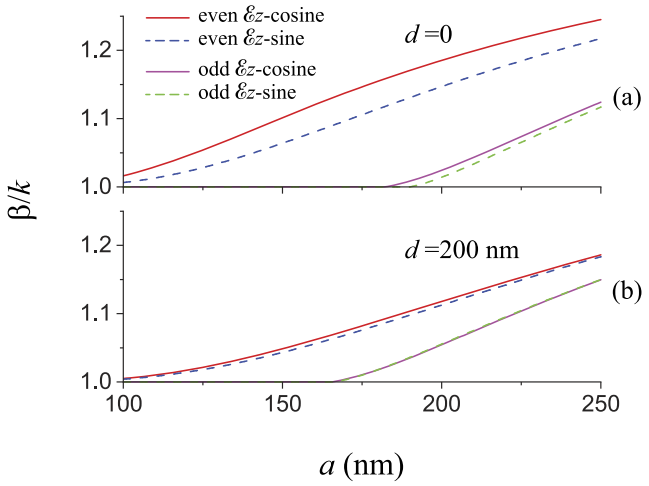

Figure 2. Propagation constant β, normalized to the free-space wave number k, as a function of the fiber radius a for two identical nanofibers. The wavelength of light is $\lambda = 800$ nm and the separation distance between the two fibers is $d = 0$ (a) and 200 nm (b). The refractive index of the fibers is $n_f = 1.4533$ and that of the surrounding medium is $n_0 = 1$.

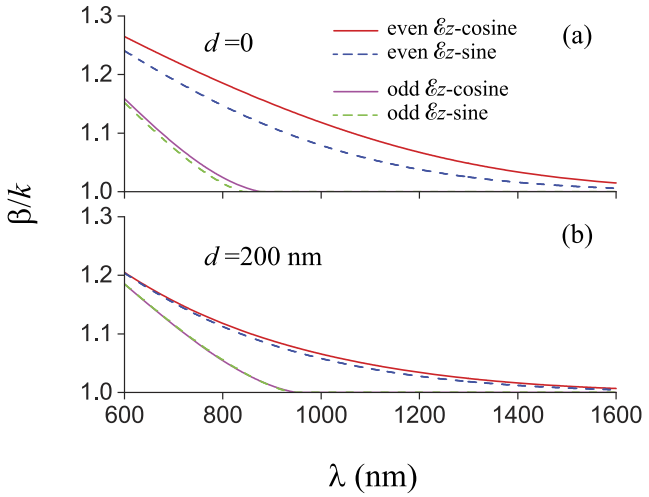

Figure 3. Propagation constant β, normalized to the free-space wave number k, as a function of the wavelength λ of light for two identical nanofibers. The fiber radius is $a = 200$ nm and the separation distance between the two fibers is $d = 0$ (a) and 200 nm (b). The refractive index n_f of the nanofibers is calculated from the four-term Sellmeier formula for fused silica [39, 40] and that of the surrounding medium is $n_0 = 1$.

figures 2–4). When the propagation constant β of an odd mode achieves the free space value k, the mode is not guided, and a cutoff is observed. We note that the position of the cutoff is determined by the solution to the equation $\beta = k$, where the propagation constant lies on the free-space light line. We recognize that the above qualitative physical explanation is partly based on the CMT, which is not valid below the cutoff. Near the cutoff, the deviation of this theory from the exact theory is significant but not dramatic (see subsection 3.3).

Comparison between figures 2(a) and (b) and between figures 3(a) and (b) shows that the cutoff values of the fiber radius a and the light wavelength λ for the odd $\mathcal{E}_z$-cosine and $\mathcal{E}_z$-sine modes depend on the separation distance d between the two fibers. A smaller d leads to a larger cutoff value of the fiber radius a and to a smaller cutoff value of the light wavelength λ. We see from figure 4(a) that, if the fiber radius a is large enough or, equivalently, the light wavelength is small enough, there is no cutoff of the guided normal modes. However, figures 4(b) and (c) show that, if the fiber radius a is small enough or, equivalently, the light wavelength is large enough, a cutoff of an odd guided normal mode may appear at a nonzero fiber separation distance d. Comparing the solid and dashed curves of figures 2–4 shows that the difference between the propagation constants of the $\mathcal{E}_z$-cosine and $\mathcal{E}_z$-sine modes reduces with increasing fiber separation distance d. This feature is due to the fact that the difference between the propagation constants

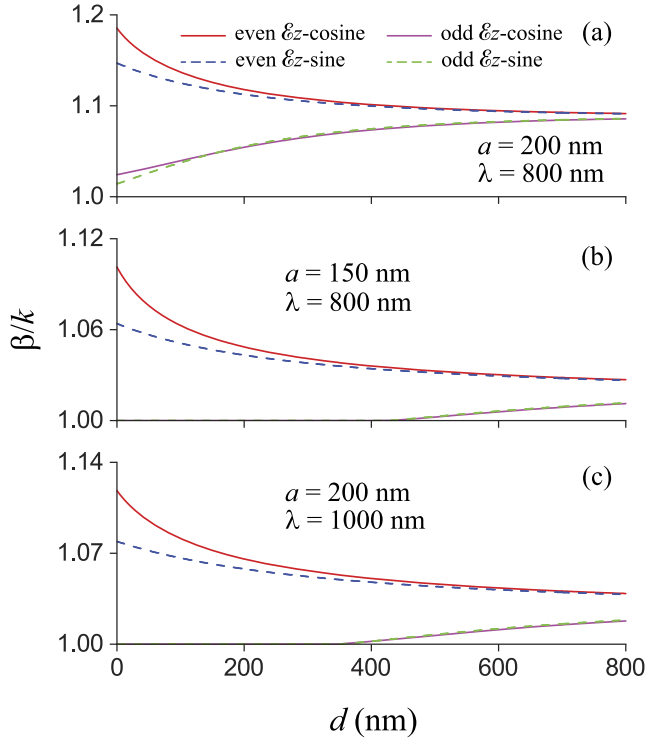

Figure 4. Propagation constant β, normalized to the free-space wave number k, as a function of the fiber separation distance d for two identical nanofibers. The fiber radius and the light wavelength are (a) $a = 200$ nm and $\lambda = 800$ nm, (b) $a = 150$ nm and $\lambda = 800$ nm, and (c) $a = 200$ nm and $\lambda = 1000$ nm. Other parameters are as in figures 2 and 3.

of the x- and y-polarized array modes is determined by the coupling between the nanofibers, which depends on the mode overlap and consequently reduces with increasing d.

Nanofibers are effective media for nonlinear optics due to the tight confinement of the fields in their guided modes [5–7, 41, 42]. The control of dispersion properties of tapered fibers has led to many interesting applications such as supercontinuum generation [41] and photon triplet generation [42]. An advantage of the system of two coupled nanofibers is that the dispersion properties of the array modes depend on not only the fiber radius, the wavelength of light, and the material refractive index but also the separation distance between the fibers. Consequently, one can control and manipulate nonlinear processes by varying the fiber separation distance in addition to the other parameters.

3.2. Spatial profiles of the fields in the guided normal modes of two identical nanofibers

In this subsection, we study the spatial distributions of the fields in the guided normal modes of two identical nanofibers. We display the cross-sectional profiles of the electric intensity distributions $|\boldsymbol{\mathcal{E}}|^2$ for different guided array modes. We also show the dependencies of the components $\mathcal{E}_x$, $\mathcal{E}_y$, and $\mathcal{E}_z$ and the intensity $|\boldsymbol{\mathcal{E}}|^2$ of the electric field on the x and y coordinates (since $\mathcal{E}_x$ and $\mathcal{E}_y$ are imaginary-valued and $\mathcal{E}_z$ is real-valued, we plot $\mathrm{Im}\,(\mathcal{E}_x) = -\mathrm{i}\mathcal{E}_x$, $\mathrm{Im}\,(\mathcal{E}_y) = -\mathrm{i}\mathcal{E}_y$, and $\mathrm{Re}\,(\mathcal{E}_z) = \mathcal{E}_z$).

3.2.1. Even $\mathcal{E}_z$-cosine mode

In figure 5, we plot the cross-sectional profile of the electric intensity distribution $|\boldsymbol{\mathcal{E}}|^2$ of the field in the even $\mathcal{E}_z$-cosine mode of two identical parallel nanofibers. The figure shows that the electric field intensity is dominant in the area between the fibers. This feature can be used to attract atoms [34–36] using a single red-detuned array-mode light field. We note that the intensity distribution of the even $\mathcal{E}_z$-cosine mode is similar to that of the perpendicular-polarization symmetric mode of a slot nanofiber, where high intensities can be realized in the vacuum region between the slot walls [20].

We show in figure 6 the dependencies of the components $\mathcal{E}_x$, $\mathcal{E}_y$, and $\mathcal{E}_z$ and the intensity $|\boldsymbol{\mathcal{E}}|^2$ of the electric field in the even $\mathcal{E}_z$-cosine mode on the x and y coordinates. Comparing the scales of the vertical axes in figure 6 shows that all the three components $\mathcal{E}_x$, $\mathcal{E}_y$, and $\mathcal{E}_z$ of the field are significant, while $\mathcal{E}_x$ (see figures 6(a) and (e)) is dominant. These features are in agreement with the fact that, in the case of single fibers, the $\mathcal{E}_z$-cosine modes are quasilinearly polarized along the x axis [1–3].

Figures 5 and 6 show that a significant portion of the field is in the outside of the nanofibers. The figures also show that abrupt changes of the fields occur at the surfaces of the fibers. Such dramatic changes arise

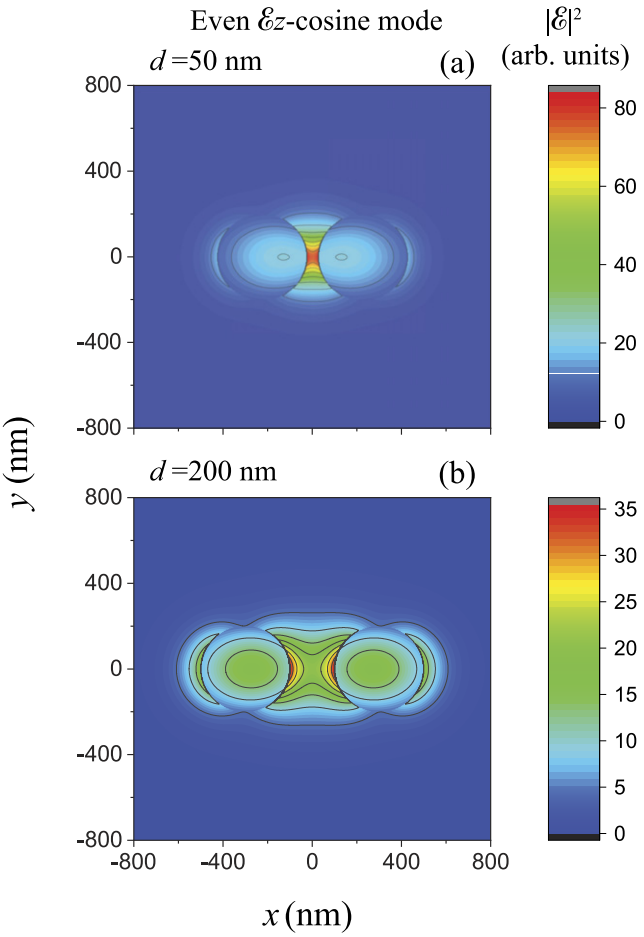

Figure 5. Cross-sectional profile of the electric intensity distribution $|\boldsymbol{\mathcal{E}}|^2$ of the field in the even $\mathcal{E}_z$-cosine mode of two identical parallel nanofibers. The fiber radius is $a = 200$ nm and the separation distance between the two fibers is $d = 50$ nm (a) and 200 nm (b). The power of light is the same in the two cases. Other parameters are as in figure 2.

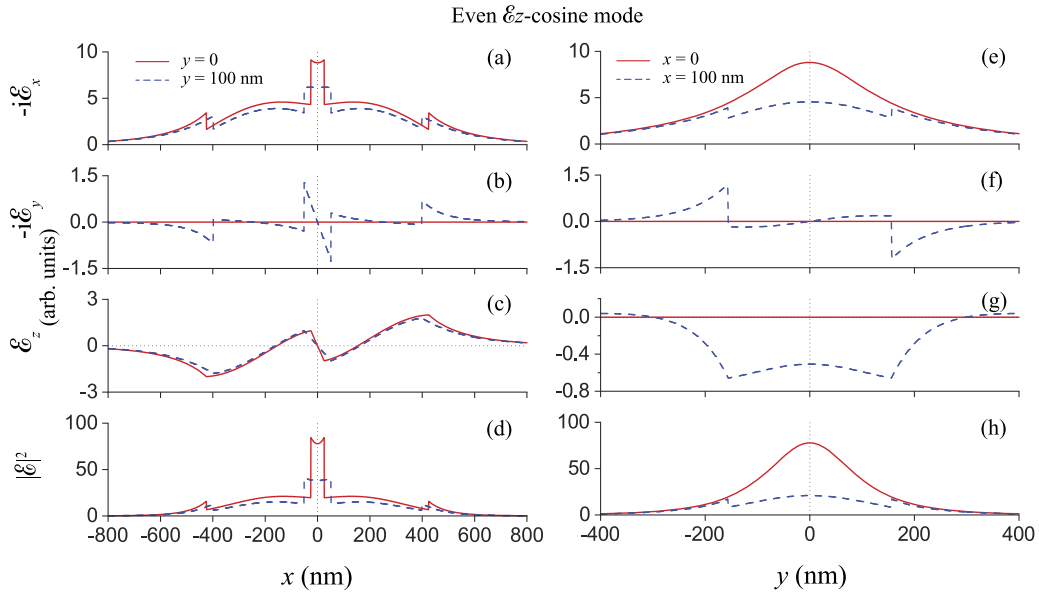

Figure 6. Dependencies of the components $\mathcal{E}_x$, $\mathcal{E}_y$, and $\mathcal{E}_z$ and the intensity $|\boldsymbol{\mathcal{E}}|^2$ of the electric field in the even $\mathcal{E}_z$-cosine mode of two identical fibers on the x and y coordinates. The fiber radius is $a = 200$ nm and the separation distance between the two fibers is $d = 50$ nm. The parameters used are the same as for figure 5(a).

from the boundary conditions and the sharp contrast between the refractive index n_f of the silica nanofibers and the refractive index $n_0 = 1$ of the vacuum medium outside the nanofibers.

The solid curve of figure 6(d) shows that the peaks of the intensity distribution occur at the facing points $(x, y) = (\pm d/2, 0)$. Meanwhile, the center $(x, y) = (0, 0)$ of the two-fiber system is a saddle point

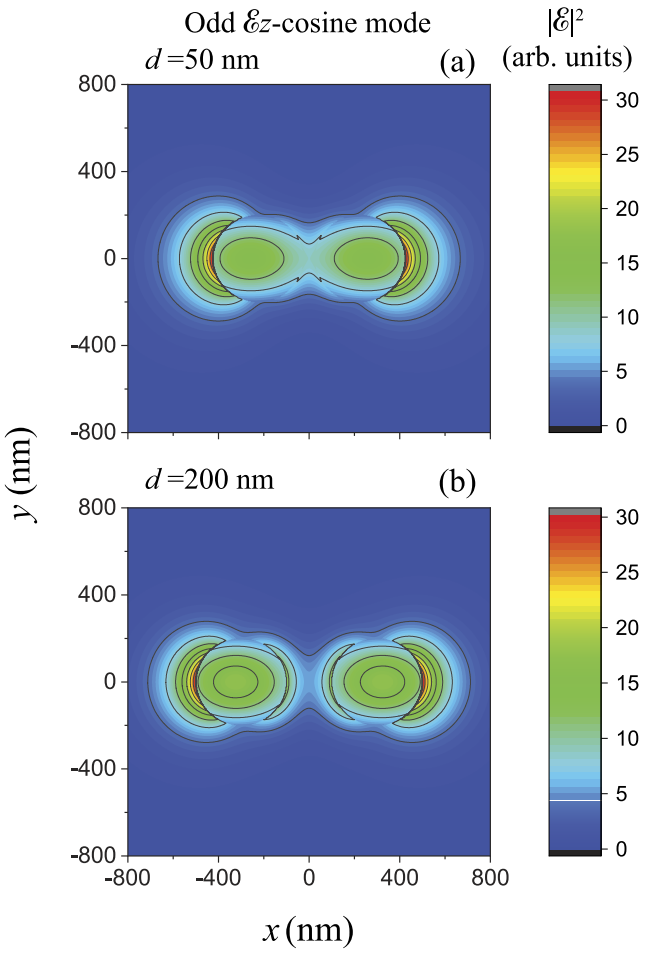

Figure 7. Cross-sectional profile of the electric intensity distribution $|\boldsymbol{\mathcal{E}}|^2$ of the field in the odd $\mathcal{E}_z$-cosine mode of two identical parallel nanofibers. The parameters used are the same as for figure 5.

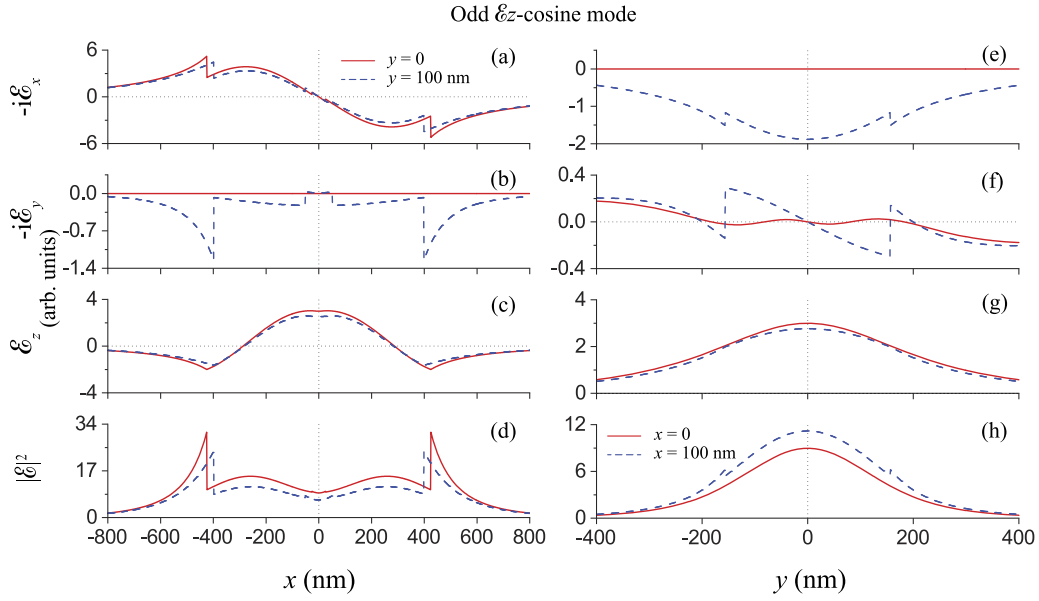

Figure 8. Dependencies of the components $\mathcal{E}_x$, $\mathcal{E}_y$, and $\mathcal{E}_z$ and the intensity $|\boldsymbol{\mathcal{E}}|^2$ of the electric field in the odd $\mathcal{E}_z$-cosine mode of two identical fibers on the x and y coordinates. The fiber radius is $a = 200$ nm and the separation distance between the two fibers is $d = 50$ nm. The parameters used are the same as for figure 7(a).

(see figures 6(d) and (h)). Despite these facts, the electric field intensity in the area between the two fibers is substantially higher than that in the surrounding area. This behavior of the electric field intensity distribution can, as already mentioned above, be used to attract atoms using red-detuned light to produce an attractive optical dipole potential.

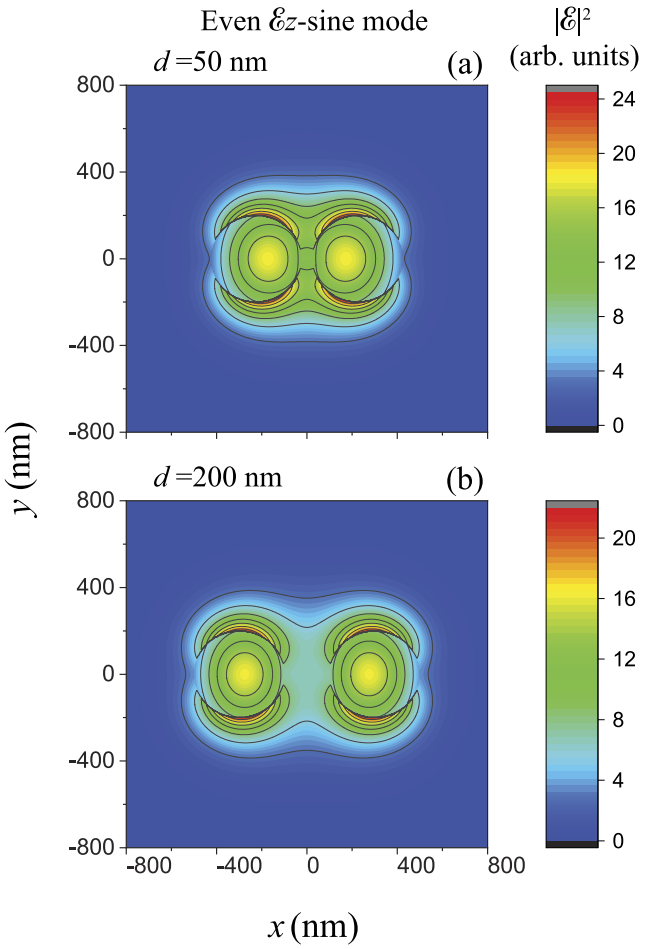

Figure 9. Cross-sectional profile of the electric intensity distribution $|\boldsymbol{\mathcal{E}}|^2$ of the field in the even $\mathcal{E}_z$-sine mode of two identical parallel nanofibers. The parameters used are the same as for figure 5.

3.2.2. Odd $\mathcal{E}_z$-cosine mode

We depict in figure 7 the cross-sectional profile of the electric intensity distribution $|\boldsymbol{\mathcal{E}}|^2$ of the field in the odd $\mathcal{E}_z$-cosine mode of two identical parallel nanofibers. We observe that the electric field intensity is dominant in the outer vicinities of the left-side surface of the left-side fiber and the right-side surface of the right-side fiber.

We display in figure 8 the dependencies of the components $\mathcal{E}_x$, $\mathcal{E}_y$, and $\mathcal{E}_z$ and the intensity $|\boldsymbol{\mathcal{E}}|^2$ of the electric field in the odd $\mathcal{E}_z$-cosine mode on the x and y coordinates. We see from the scales of the vertical axes in figure 8 that all the three components $\mathcal{E}_x$, $\mathcal{E}_y$, and $\mathcal{E}_z$ of the field are significant.

3.2.3. Even $\mathcal{E}_z$-sine mode

We show in figure 9 the cross-sectional profile of the electric intensity distribution $|\boldsymbol{\mathcal{E}}|^2$ of the field in the even $\mathcal{E}_z$-sine mode of two identical parallel nanofibers. The figure shows that the electric field intensity is dominant in the outer vicinities of the top and bottom parts of the surfaces of the fibers, and is significant in the area between the fiber surfaces.

In figure 10, the dependencies of the components $\mathcal{E}_x$, $\mathcal{E}_y$, and $\mathcal{E}_z$ and the intensity $|\boldsymbol{\mathcal{E}}|^2$ of the electric field in the even $\mathcal{E}_z$-sine mode on the x and y coordinates are plotted. We see from the scales of the vertical axes in figure 10 that all the three components $\mathcal{E}_x$, $\mathcal{E}_y$, and $\mathcal{E}_z$ of the field are significant, while $\mathcal{E}_y$ (see figures 10(b) and (f)) is dominant. These features are in agreement with the fact that, in the case of single fibers, the $\mathcal{E}_z$-sine modes are quasilinearly polarized along the y axis [1–3].

3.2.4. Odd $\mathcal{E}_z$-sine mode

The cross-sectional profile of the electric intensity distribution $|\boldsymbol{\mathcal{E}}|^2$ of the field in the odd $\mathcal{E}_z$-sine mode of two identical parallel nanofibers is displayed in figure 11. We observe that the electric field intensity is dominant in the vicinities of the top and bottom parts of the surfaces of the fibers, and is significant in the outer vicinities of the left-side surface of the left-side fiber and the right-side surface of the right-side fiber.

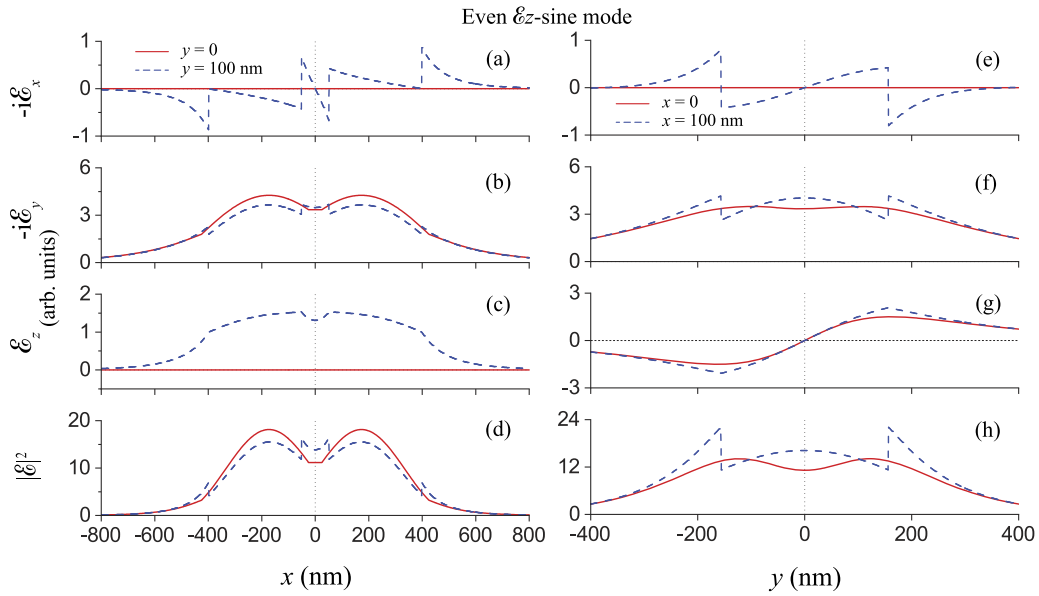

Figure 10. Dependencies of the components $\mathcal{E}_x$, $\mathcal{E}_y$, and $\mathcal{E}_z$ and the intensity $|\boldsymbol{\mathcal{E}}|^2$ of the electric field in the even $\mathcal{E}_z$-sine mode of two identical fibers on the x and y coordinates. The fiber radius is $a = 200$ nm and the separation distance between the two fibers is $d = 50$ nm. The parameters used are the same as for figure 9(a).

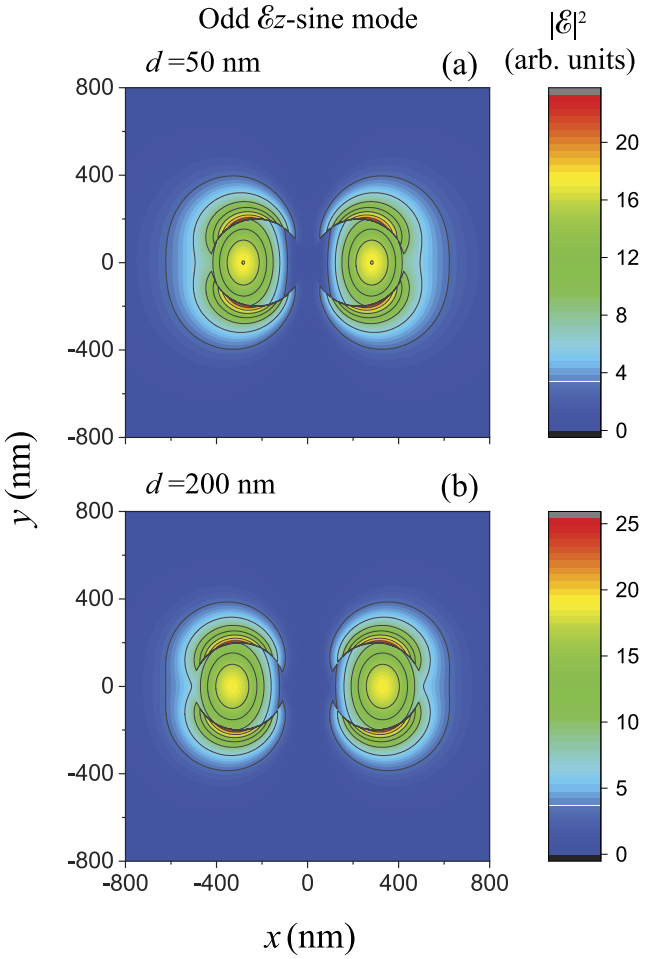

Figure 11. Cross-sectional profile of the electric intensity distribution $|\boldsymbol{\mathcal{E}}|^2$ of the field in the odd $\mathcal{E}_z$-sine mode of two identical parallel nanofibers. The parameters used are the same as for figure 5.

We plot in figure 12 the dependencies of the components $\mathcal{E}_x$, $\mathcal{E}_y$, and $\mathcal{E}_z$ and the intensity $|\boldsymbol{\mathcal{E}}|^2$ of the electric field in the odd $\mathcal{E}_z$-sine mode on the x and y coordinates. We see from the scales of the vertical axes in figure 12 that all the three components $\mathcal{E}_x$, $\mathcal{E}_y$, and $\mathcal{E}_z$ of the field are significant.

Figure 11 and the solid curves of figures 12(d) and (h) confirm the prediction that the electric field of the odd $\mathcal{E}_z$-sine mode at the two-fiber center $(x, y) = (0, 0)$ is zero. This feature of the odd $\mathcal{E}_z$-sine mode can

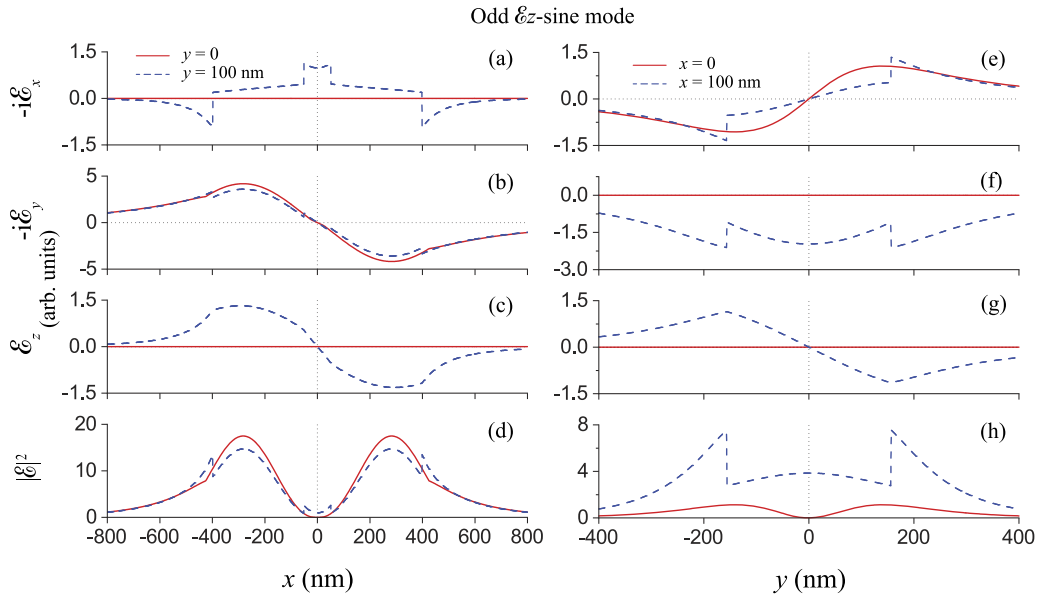

Figure 12. Dependencies of the components $\mathcal{E}_x$, $\mathcal{E}_y$, and $\mathcal{E}_z$ and the intensity $|\boldsymbol{\mathcal{E}}|^2$ of the electric field in the odd $\mathcal{E}_z$-sine mode of two identical fibers on the x and y coordinates. The fiber radius is $a = 200$ nm. The fiber separation distance is $d = 50$ nm. The parameters used are the same as for figure 11(a).

be used to trap ground-state atoms with a blue-detuned optical dipole potential [34–36], or to trap Rydberg atoms with a ponderomotive optical Rydberg-electron potential [37, 38]. We emphasize that the existence of a local minimum of exact zero at the two-fiber center is a specific property of the intensity of the electric field in the odd $\mathcal{E}_z$-sine mode, and occurs for any fiber separation distance d. To reduce to effects of the fiber surfaces on the atoms at the two-fiber center, we can increase the separation between the fibers.

A common feature of figures 5, 7, 9 and 11 is that the field intensity $|\boldsymbol{\mathcal{E}}|^2$ is symmetric with respect to the principal axes x and y. This symmetry is an obvious consequence of the geometry of the system of two identical parallel nanofibers.

We note that the symmetry properties of the field components $\mathcal{E}_x$, $\mathcal{E}_y$, and $\mathcal{E}_z$, shown in figures 6, 8, 10 and 12, are in agreement with equations (8)–(11) and tables 1 and 2. In particular, the symmetry properties of the curves for the field components in the left panel of figure 6 (for the even $\mathcal{E}_z$-cosine mode) with respect to the coordinate x are the same as those of the corresponding curves in the left panel of figure 12 (for the odd $\mathcal{E}_z$-sine mode) and are opposite to those of the corresponding curves in the left panels of figure 8 (for the odd $\mathcal{E}_z$-cosine mode) and figure 10 (for the even $\mathcal{E}_z$-sine mode). Meanwhile, the symmetry properties of the curves for the field components in the right panel of figure 6 (for the even $\mathcal{E}_z$-cosine mode) with respect to the coordinate y are the same as those of the corresponding curves in the right panel of figure 8 (for the odd $\mathcal{E}_z$-cosine mode) and are opposite to those of the corresponding curves in the right panels of figure 10 (for the even $\mathcal{E}_z$-sine mode) and figure 12 (for the odd $\mathcal{E}_z$-sine mode).

It is worth emphasizing that the electric intensity of the even $\mathcal{E}_z$-cosine mode is dominant in the area between the fibers while the electric intensity of the odd $\mathcal{E}_z$-sine mode attains a local minimum of exactly zero at the two-fiber center. These features may be used to attract atoms with a red-detuned light field in the even $\mathcal{E}_z$-cosine mode or a blue-detuned light field in the odd $\mathcal{E}_z$-sine mode. We note that the effects of the van der Waals potential on the trapping of atoms must be considered. In addition, it is challenging to excite a single array mode of the two coupled nanofibers. These issues deserve separate studies.

Comparison between figures 5 and 7 and between figures 9 and 11 shows that, in the region between the two nanofibers, the interference between the fields of the individual nanofibers is constructive for even modes (see figures 5 and 9) and destructive for odd modes (see figures 7 and 11). Thus, the even and odd modes behave like the bright and dark states of a three-level atom interacting with two driving light fields [43]. This observation is consistent with the results of the CMT [1–3].

3.3. Comparison between the exact mode theory and the coupled mode theory

From the CMT [1–3], the coupling length for the fiber modes with the principal polarization $p = x, y$ of two parallel fibers is $L_p = \pi/2\eta_p$, where $\eta_p = (\kappa_p - c_p\chi_p)/(1 - c_p^2)$ is the power transfer coefficient. Here, κ_p, χ_p, and c_p are the coefficients of directional coupling, self coupling, and butt coupling, respectively. The calculations of the power transfer coefficient η_p for two parallel nanofibers have been reported in [22].

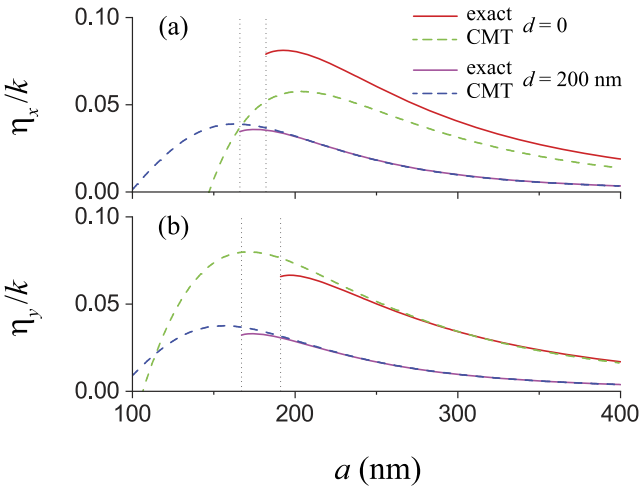

Figure 13. Power transfer coefficients η_x (a) and η_y (b) between two identical fibers calculated from the exact theory for the guided array modes (solid lines) and the coupled mode theory (dashed lines) as functions of the fiber radius a for the fiber separation distances $d = 0$ and 200 nm. The light wavelength is $\lambda = 800$ nm. Other parameters are as in figure 2. The vertical dashed lines indicate the positions of the cutoffs of the odd array modes.

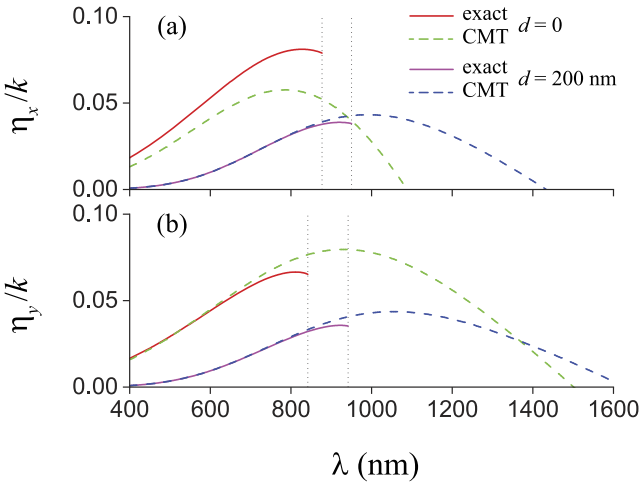

Figure 14. Power transfer coefficients η_x (a) and η_y (b) between two identical fibers calculated from the exact theory for the guided array modes (solid lines) and the coupled mode theory (dashed lines) as functions of the light wavelength λ for the fiber separation distances $d = 0$ and 200 nm. The fiber radius is $a = 200$ nm. Other parameters are as in figure 3. The vertical dashed lines indicate the positions of the cutoffs of the odd array modes.

In the framework of the coupled mode theory [1–3], the transfer of power between the coupled fibers is a result of the beating between two normal modes. The power transfer coefficient is $\eta_p = (\beta_a^{(p)} - \beta_b^{(p)})/2$, where $\beta_a^{(p)}$ and $\beta_b^{(p)}$ are the propagation constants of the normal modes a and b with the principal polarization $p = x$ or y (the $\mathcal{E}_z$-cosine or $\mathcal{E}_z$-sine type). For two identical nanofibers, the normal modes a and b are the even ($\nu = -1$) and odd ($\nu = 1$) modes, respectively. Hence, the power transfer coefficient η_p can be calculated from the exact theory for the guided array modes [23].

We plot in figures 13–15 the power transfer coefficients η_x and η_y between two identical fibers calculated from the exact theory for the guided array modes (solid curves) and the coupled mode theory (dashed curves) as functions of the fiber radius a, the light wavelength λ, and the fiber separation distance d. In these figures, the vertical dashed lines indicate the positions of the cutoffs of the odd array modes that occur in the framework of the exact theory when d is small and either a is small or λ is large in the ranges plotted. The coupled mode theory is not able to predict the mode cutoffs. Below a cutoff, the overlap between the modes of the different individual fibers is so significant that only even array modes exist. In this regime, the concept of power transfer between the fibers becomes meaningless and, hence, the coupled mode theory is not valid.

Thus, when the fiber separation distance is too small and either the fiber radius is too small or the wavelength of light is too large, the two nanofibers cannot be considered as independent or weakly coupled

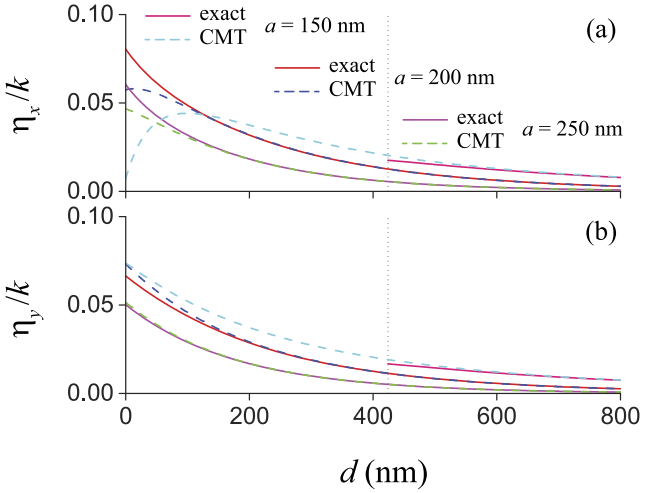

Figure 15. Power transfer coefficients η_x (a) and η_y (b) between two identical fibers calculated from the exact theory for the guided array modes (solid lines) and the coupled mode theory (dashed lines) as functions of the fiber separation distance d for the fiber radii $a = 150$, 200, and 250 nm. The light wavelength is $\lambda = 800$ nm. Other parameters are as in figure 2. The vertical dashed lines indicate the positions of the cutoffs of the odd array modes.

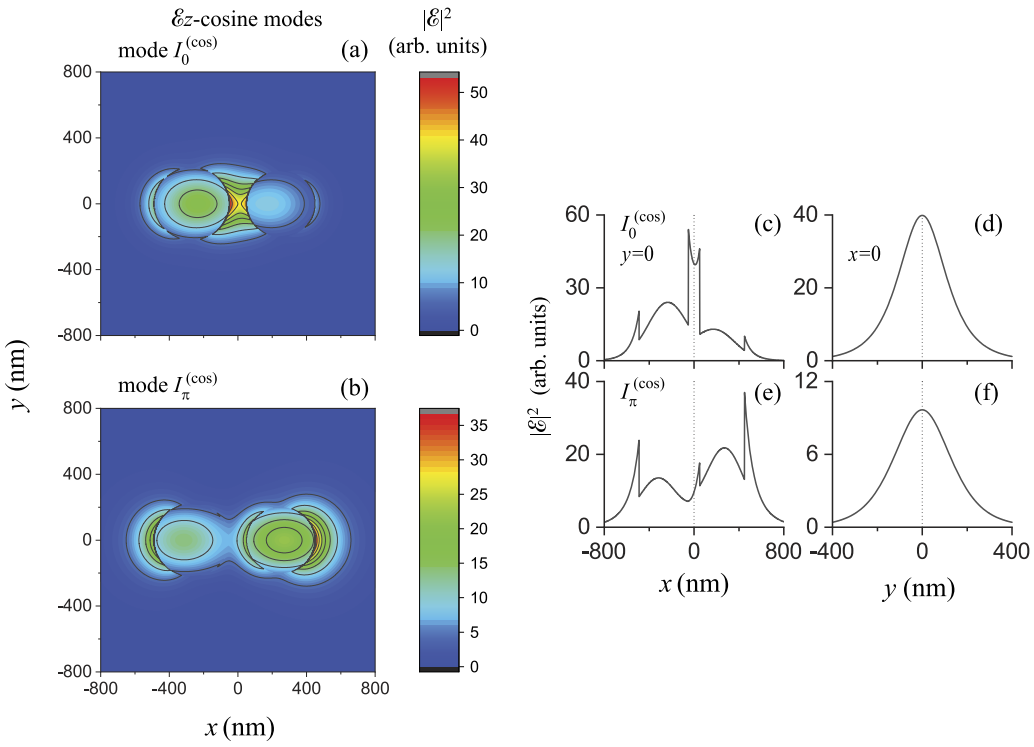

Figure 16. Left panel: cross-sectional profiles of the electric intensity distributions $|\boldsymbol{\mathcal{E}}|^2$ of the fields in the $\mathcal{E}_z$-cosine modes $I_0^{(\cos)}$ and $I_\pi^{(\cos)}$ of two nonidentical parallel nanofibers. Right panel: dependencies of the intensities $|\boldsymbol{\mathcal{E}}|^2$ of the fields in the modes on the x and y coordinates. The fiber radii are $a_1 = 220$ nm and $a_2 = 200$ nm. The fiber separation distance is $d = 100$ nm. Other parameters are as in figure 2.

waveguides. In this case, only two even-type principal array modes can be supported (like for a single nanofiber). This condition also marks the limits of validity for the coupled mode theory, which assumes weak coupling.

We observe from figures 13–15 that the results of the coupled mode theory agree well with those of the exact theory in the far-above-cutoff regions where the fiber radius is large, the wavelength of light is small, or the fiber separation distance is large. Near to a cutoff, the differences between the results of the exact and coupled mode theories are significant but not dramatic. For touching nanofibers ($d = 0$), the differences between the results of the two theories become large when the fiber radius a is small (see figure 13) or the light wavelength λ is large (see figure 14). Comparison between figures 13(a) and (b) and between

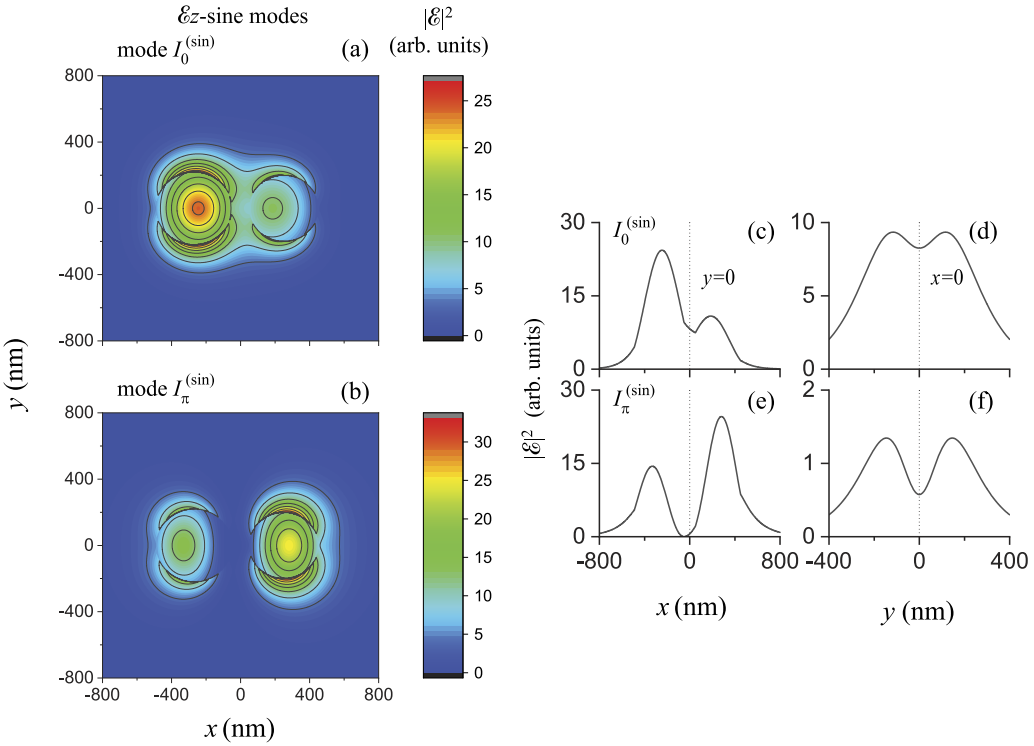

Figure 17. Left panel: cross-sectional profiles of the electric intensity distributions $|\boldsymbol{\mathcal{E}}|^2$ of the fields in the $\mathcal{E}_z$-sine modes $I_0^{(\sin)}$ and $I_\pi^{(\sin)}$ of two nonidentical parallel nanofibers. Right panel: dependencies of the intensities $|\boldsymbol{\mathcal{E}}|^2$ of the fields in the modes on the x and y coordinates. The parameters used are the same as for figure 16.

figures 14(a) and (b) shows that, for touching nanofibers, the differences between the results of the two theories for the x-polarized modes are larger than those for the y-polarized modes.

3.4. Nonidentical nanofibers

It is desirable to know the effects of a difference between the radii of the nanofibers on the properties of the guided normal modes and the symmetry of the field intensity distributions. When the two nanofibers are not identical, the symmetry relations (8) and (9) for the x coordinate are not valid and, hence, the guided array modes cannot be identified as even and odd modes anymore. We follow [23] and label the first two modes of the $\mathcal{E}_z$-sine type as $I_0^{(\sin)}$ and $I_\pi^{(\sin)}$. Similarly, we label the first two modes of the $\mathcal{E}_z$-cosine type as $I_0^{(\cos)}$ and $I_\pi^{(\cos)}$. Like the case of identical nanofibers, modes $I_0^{(\sin)}$ and $I_0^{(\cos)}$ have no cutoff, while modes $I_\pi^{(\sin)}$ and $I_\pi^{(\cos)}$ may have cutoffs. Note that the symmetry relations (10) and (11) for the y coordinate remain valid for nonidentical nanofibers.

In the left panel of figure 16 the cross-sectional profiles of the electric intensity distributions $|\boldsymbol{\mathcal{E}}|^2$ of the fields in the $\mathcal{E}_z$-cosine modes of two nonidentical parallel nanofibers are plotted. We show in the right panel of figure 16 the dependencies of $|\boldsymbol{\mathcal{E}}|^2$ on the x and y coordinates. The corresponding results for the $\mathcal{E}_z$-sine modes are shown in figure 17. We observe from the figures that the intensity distribution $|\boldsymbol{\mathcal{E}}|^2$ is asymmetric with respect to the coordinate x and symmetric with respect to the coordinate y. These properties are obvious consequences of the geometry of the system of two nonidentical parallel nanofibers.

Figures 16(a), (c) and (d) show that the electric field intensity of the $I_0^{(\cos)}$ mode is dominant in the area between the nanofibers and, hence, atoms can be attracted to this area using a single red-detuned light field. We observe from figures 17(b) and (e) that the electric field intensity of the $I_\pi^{(\sin)}$ mode has a local minimum of exact zero at a point on the x axis in the region between the nanofibers and, hence, atoms can be attracted to this area using a single blue-detuned light field.

Figures 16 and 17 show that, in the cases of $I_0^{(\cos,\sin)}$ modes, the intensity of the field in the area of the bigger nanofiber (nanofiber 1) is higher than that in the area of the smaller nanofiber (nanofiber 2). Meanwhile, in the cases of $I_\pi^{(\cos,\sin)}$ modes, the intensity of the field in the area of the smaller nanofiber (nanofiber 2) is higher than that in the area of the bigger nanofiber (nanofiber 1). We see that a slight difference between the radii of the nanofibers ($a_1 = 220$ nm and $a_2 = 200$ nm) leads to strong asymmetry of the intensity distributions of the guided normal modes. This feature is a consequence of the fact that the dependencies of the coupling between the nanofibers on the fiber radii are nonlinear.

4. Summary

We have studied the cross-sectional profiles and spatial distributions of the fields in guided normal modes of two coupled parallel optical nanofibers. We have shown that the distributions of the components of the field in a guided normal mode of two identical nanofibers are either symmetric or antisymmetric with respect to the radial principal axis x and the tangential principal axis y in the cross-sectional plane of the fibers. The symmetry of the magnetic field components with respect to the principal axes is opposite to that of the electric field components. We have found that, in the case of even $\mathcal{E}_z$-cosine modes, the electric intensity distribution is dominant in the area between the fibers, with a saddle point at the two-fiber center. This feature may be used to attract atoms with a single red-detuned guided normal-mode light field. Meanwhile, in the case of odd $\mathcal{E}_z$-sine modes, the electric intensity distribution at the two-fiber center attains a local minimum of exactly zero. This feature may be used to trap atoms with a single blue-detuned guided normal-mode light field. We have observed that the differences between the results of the coupled mode theory and the exact theory are large when the separation distance between the two fibers is small and either the radius of the fibers is small or the wavelength of light is large. We have shown that, in the case where the two nanofibers are not identical, the intensity distribution is, due to the geometry of the system, symmetric about the radial principal axis x but asymmetric about the tangential principal axis y. We have found that a slight difference between the radii of the nanofibers leads to strong asymmetry of the intensity distributions of the guided normal modes. Potential uses of the fields in guided normal modes of two coupled parallel nanofibers for trapping, guiding, and probing atoms deserve further systematic investigations.

Acknowledgments

This work was supported by the Okinawa Institute of Science and Technology Graduate University.

Data availability statement

All data that support the findings of this study are included within the article (and any supplementary files).

Appendix A. Equations for the expansion coefficients of the array modes

In this appendix, we summarize the key results of [23].

According to [23], the longitudinal components $\mathcal{E}_z$ and $\mathcal{H}_z$ of the electric and magnetic parts, respectively, of the field in a guided normal mode are given by equations (1) and (2). Since we consider only guided (bound) modes, equations (2) do not contain the Hankel functions and the modified Bessel functions of the first kind.

The Cartesian-coordinate transverse components $\mathcal{E}_{x,y}$ and $\mathcal{H}_{x,y}$ of the field are given by equations (4). In an arbitrary polar coordinate system (r, φ) of the transverse plane, the radial components $\mathcal{E}_r$ and $\mathcal{H}_r$ and the azimuthal components $\mathcal{E}_\varphi$ and $\mathcal{H}_\varphi$ of the field are given as [1–3]

$$\begin{aligned}
\mathcal{E}_r &= \frac{\mathrm{i}\beta}{k^2 n_{\mathrm{ref}}^2 - \beta^2}\left(\frac{\partial}{\partial r}\mathcal{E}_z + \frac{\omega\mu_0}{\beta}\frac{\partial}{r\partial\varphi}\mathcal{H}_z\right),\\
\mathcal{E}_\varphi &= \frac{\mathrm{i}\beta}{k^2 n_{\mathrm{ref}}^2 - \beta^2}\left(\frac{\partial}{r\partial\varphi}\mathcal{E}_z - \frac{\omega\mu_0}{\beta}\frac{\partial}{\partial r}\mathcal{H}_z\right),\\
\mathcal{H}_r &= \frac{\mathrm{i}\beta}{k^2 n_{\mathrm{ref}}^2 - \beta^2}\left(\frac{\partial}{\partial r}\mathcal{H}_z - \frac{\omega\epsilon_0 n_{\mathrm{ref}}^2}{\beta}\frac{\partial}{r\partial\varphi}\mathcal{E}_z\right),\\
\mathcal{H}_\varphi &= \frac{\mathrm{i}\beta}{k^2 n_{\mathrm{ref}}^2 - \beta^2}\left(\frac{\partial}{r\partial\varphi}\mathcal{H}_z + \frac{\omega\epsilon_0 n_{\mathrm{ref}}^2}{\beta}\frac{\partial}{\partial r}\mathcal{E}_z\right).
\end{aligned} \tag{A.1}$$

Like equations (4), equations (A.1) are consequences of the Maxwell equations and the translational symmetry of the system in the z direction. It is clear that the radial components $\mathcal{E}_{r_j}$ and $\mathcal{H}_{r_j}$ and the azimuthal components $\mathcal{E}_{\varphi_j}$ and $\mathcal{H}_{\varphi_j}$ of the field in the local fiber-based polar coordinate system $\{r_j, \varphi_j\}$ can be calculated from the longitudinal components $\mathcal{E}_z$ and $\mathcal{H}_z$ using equations (A.1) for $\{r, \varphi\} = \{r_j, \varphi_j\}$. Equations (A.1) allow us to work straightforwardly with the boundary conditions for the individual circular fibers.

The boundary conditions for the axial components $\mathcal{E}_z$ and $\mathcal{H}_z$ and the local-fiber-coordinate azimuthal components $\mathcal{E}_{\varphi_j}$ and $\mathcal{H}_{\varphi_j}$ of the electric and magnetic fields at the surface S_j of fiber j read

$$\begin{aligned} \mathcal{E}_z|_{S_j^-} &= \mathcal{E}_z|_{S_j^+}, \qquad \mathcal{H}_z|_{S_j^-} = \mathcal{H}_z|_{S_j^+}, \\ \mathcal{E}_{\varphi_j}|_{S_j^-} &= \mathcal{E}_{\varphi_j}|_{S_j^+}, \qquad \mathcal{H}_{\varphi_j}|_{S_j^-} = \mathcal{H}_{\varphi_j}|_{S_j^+}, \end{aligned} \tag{A.2}$$

where the symbols S_j^- and S_j^+ indicate the inner and outer sides of the surface of fiber j.

To apply the boundary conditions at the surface of nanofiber j, we express $\mathcal{E}_z$ and $\mathcal{H}_z$ outside the fibers as functions of r_j and φ_j using the Graf's and Gegenbauer's addition theorem [44]. According to this theorem, we have

$$\begin{aligned} K_n(qr_2)\begin{pmatrix}\cos n\theta_2\\ \sin n\theta_2\end{pmatrix} &= \sum_{m=-\infty}^{+\infty} K_{n+m}(qW)I_m(qr_1)\begin{pmatrix}\cos m\theta_1\\ \sin m\theta_1\end{pmatrix}, \\ K_n(qr_1)\begin{pmatrix}\cos n\theta_1\\ \sin n\theta_1\end{pmatrix} &= \sum_{m=-\infty}^{+\infty} K_{n+m}(qW)I_m(qr_2)\begin{pmatrix}\cos m\theta_2\\ \sin m\theta_2\end{pmatrix}, \end{aligned} \tag{A.3}$$

where $r_1 = PO_1$, $r_2 = PO_2$, $W = O_1O_2$, $\theta_1 = \angle PO_1O_2 = \varphi_1$, and $\theta_2 = \angle PO_2O_1 = \pi - \varphi_2$ (see figure 1).

For the $\mathcal{E}_z$-cosine modes, the expansion coefficients E_{nj}, F_{nj}, G_{nj}, and H_{nj} vanish. We apply the boundary conditions (A.2) to these modes. Then, we find that the coefficients A_{nj} and B_{nj} for the field inside the fibers are given by the equations

$$\begin{aligned} J_n(u_j)A_{nj} &= K_n(w_j)C_{nj} + I_n(w_j)\sum_{m=0}^{\infty} f_{jnm}C_{m\bar{j}}, \\ J_n(u_j)B_{nj} &= K_n(w_j)D_{nj} + I_n(w_j)\sum_{m=0}^{\infty} g_{jnm}D_{m\bar{j}}, \end{aligned} \tag{A.4}$$

while the coefficients C_{nj} and D_{nj} for the field outside the fibers are nonzero solutions of the equations [23]

$$\begin{aligned} &n\left(\frac{1}{u_j^2}+\frac{1}{w_j^2}\right)\left[K_n(w_j)C_{nj} + I_n(w_j)\sum_{m=0}^{\infty} f_{jnm}C_{m\bar{j}}\right] + \frac{\omega\mu_0}{\beta}\left[\frac{J_n'(u_j)}{u_jJ_n(u_j)} + \frac{K_n'(w_j)}{w_jK_n(w_j)}\right]K_n(w_j)D_{nj} \\ &\quad + \frac{\omega\mu_0}{\beta}\left[\frac{J_n'(u_j)}{u_jJ_n(u_j)} + \frac{I_n'(w_j)}{w_jI_n(w_j)}\right]I_n(w_j)\sum_{m=0}^{\infty} g_{jnm}D_{m\bar{j}} = 0, \\ &n\left(\frac{1}{u_j^2}+\frac{1}{w_j^2}\right)\left[K_n(w_j)D_{nj} + I_n(w_j)\sum_{m=0}^{\infty} g_{jnm}D_{m\bar{j}}\right] + \frac{\omega\epsilon_0}{\beta}\left[\frac{n_j^2J_n'(u_j)}{u_jJ_n(u_j)} + \frac{n_0^2K_n'(w_j)}{w_jK_n(w_j)}\right]K_n(w_j)C_{nj} \\ &\quad + \frac{\omega\epsilon_0}{\beta}\left[\frac{n_j^2J_n'(u_j)}{u_jJ_n(u_j)} + \frac{n_0^2I_n'(w_j)}{w_jI_n(w_j)}\right]I_n(w_j)\sum_{m=0}^{\infty} f_{jnm}C_{m\bar{j}} = 0. \end{aligned} \tag{A.5}$$

Here, we have introduced the notation $\bar{j} = 2$ or 1 for $j = 1$ or 2, respectively. We have also introduced the parameters

$$u_j = h_ja_j, \qquad w_j = qa_j, \tag{A.6}$$

and the coefficients

$$f_{1nm} = (-1)^m f_{nm}, \qquad g_{1nm} = (-1)^m g_{nm}, \tag{A.7}$$

and

$$f_{2nm} = (-1)^n f_{nm}, \qquad g_{2nm} = (-1)^n g_{nm}, \tag{A.8}$$

where

$$\begin{aligned} f_{nm} &= K_{m+n}(qW) + K_{m-n}(qW) \text{ for } n > 0, \\ f_{0,m} &= K_m(qW), \\ g_{nm} &= -K_{m+n}(qW) + K_{m-n}(qW), \end{aligned} \tag{A.9}$$

with $W = d + a_1 + a_2$ being the distance between the fiber centers.

For the $\mathcal{E}_z$-sine modes, the expansion coefficients A_{nj}, B_{nj}, C_{nj}, and D_{nj} vanish. We apply the boundary conditions (A.2) to these modes. Then, we find that the coefficients E_{nj} and F_{nj} for the field inside the fibers

are given by the equations

$$J_n(u_j)E_{nj} = K_n(w_j)G_{nj} + I_n(w_j)\sum_{m=0}^{\infty} g_{jnm}G_{m\bar{j}},$$
$$J_n(u_j)F_{nj} = K_n(w_j)H_{nj} + I_n(w_j)\sum_{m=0}^{\infty} f_{jnm}H_{m\bar{j}}, \tag{A.10}$$

while the coefficients G_{nj} and H_{nj} for the field outside the fibers are nonzero solutions of the equations [23]

$$n\left(\frac{1}{u_j^2}+\frac{1}{w_j^2}\right)\left[K_n(w_j)G_{nj} + I_n(w_j)\sum_{m=0}^{\infty} g_{jnm}G_{m\bar{j}}\right] - \frac{\omega\mu_0}{\beta}\left[\frac{J_n'(u_j)}{u_jJ_n(u_j)}+\frac{K_n'(w_j)}{w_jK_n(w_j)}\right]K_n(w_j)H_{nj}$$
$$-\frac{\omega\mu_0}{\beta}\left[\frac{J_n'(u_j)}{u_jJ_n(u_j)}+\frac{I_n'(w_j)}{w_jI_n(w_j)}\right]I_n(w_j)\sum_{m=0}^{\infty} f_{jnm}H_{m\bar{j}} = 0,$$
$$n\left(\frac{1}{u_j^2}+\frac{1}{w_j^2}\right)\left[K_n(w_j)H_{nj} + I_n(w_j)\sum_{m=0}^{\infty} f_{jnm}H_{m\bar{j}}\right] - \frac{\omega\epsilon_0}{\beta}\left[\frac{n_j^2J_n'(u_j)}{u_jJ_n(u_j)}+\frac{n_0^2K_n'(w_j)}{w_jK_n(w_j)}\right]K_n(w_j)G_{nj}$$
$$-\frac{\omega\epsilon_0}{\beta}\left[\frac{n_j^2J_n'(u_j)}{u_jJ_n(u_j)}+\frac{n_0^2I_n'(w_j)}{w_jI_n(w_j)}\right]I_n(w_j)\sum_{m=0}^{\infty} g_{jnm}G_{m\bar{j}} = 0. \tag{A.11}$$

We emphasize that equations (A.5) and (A.11) contain the mode expansion coefficients with the indices j and $\bar{j}$, where $\bar{j} = 2$ or 1 for $j = 1$ or 2, respectively. They are in agreement with the results of [23], presented in the form of 4×4 matrix minors.

We consider the particular case where the two fibers are identical, that is, the two fibers have the same radius $a_1 = a_2 = a$ and the same core refractive index $n_1 = n_2 = n_f$. In this case, we have $h_1 = h_2$, $u_1 = u_2$, and $w_1 = w_2$. Then, for the $\mathcal{E}_z$-cosine modes, we find

$$A_{m2} = (-1)^m\nu A_{m1}, \qquad B_{m2} = (-1)^m\nu B_{m1},$$
$$C_{m2} = (-1)^m\nu C_{m1}, \qquad D_{m2} = (-1)^m\nu D_{m1}, \tag{A.12}$$

and, for the $\mathcal{E}_z$-sine modes, we get

$$E_{m2} = (-1)^m\nu E_{m1}, \qquad F_{m2} = (-1)^m\nu F_{m1},$$
$$G_{m2} = (-1)^m\nu G_{m1}, \qquad H_{m2} = (-1)^m\nu H_{m1}, \tag{A.13}$$

where $\nu = -1$ or $+1$ corresponds to the even or odd mode [23]. Hence, equations (A.5) for the $\mathcal{E}_z$-cosine modes take the form [23]

$$n\left(\frac{1}{u^2}+\frac{1}{w^2}\right)\left[K_n(w)C_{n1} + I_n(w)\sum_{m=0}^{\infty}\nu f_{nm}C_{m1}\right] + \frac{\omega\mu_0}{\beta}\left[\frac{J_n'(u)}{uJ_n(u)}+\frac{K_n'(w)}{wK_n(w)}\right]K_n(w)D_{n1}$$
$$+\frac{\omega\mu_0}{\beta}\left[\frac{J_n'(u)}{uJ_n(u)}+\frac{I_n'(w)}{wI_n(w)}\right]I_n(w)\sum_{m=0}^{\infty}\nu g_{nm}D_{m1} = 0,$$
$$n\left(\frac{1}{u^2}+\frac{1}{w^2}\right)\left[K_n(w)D_{n1} + I_n(w)\sum_{m=0}^{\infty}\nu g_{nm}D_{m1}\right] + \frac{\omega\epsilon_0}{\beta}\left[\frac{n_1^2J_n'(u)}{uJ_n(u)}+\frac{n_0^2K_n'(w)}{wK_n(w)}\right]K_n(w)C_{n1}$$
$$+\frac{\omega\epsilon_0}{\beta}\left[\frac{n_1^2J_n'(u)}{uJ_n(u)}+\frac{n_0^2I_n'(w)}{wI_n(w)}\right]I_n(w)\sum_{m=0}^{\infty}\nu f_{nm}C_{m1} = 0, \tag{A.14}$$

and equations (A.11) for the $\mathcal{E}_z$-sine modes become [23]

$$n\left(\frac{1}{u^2}+\frac{1}{w^2}\right)\left[K_n(w)G_{n1} + I_n(w)\sum_{m=0}^{\infty}\nu g_{nm}G_{m1}\right] - \frac{\omega\mu_0}{\beta}\left[\frac{J_n'(u)}{uJ_n(u)}+\frac{K_n'(w)}{wK_n(w)}\right]K_n(w)H_{n1}$$
$$-\frac{\omega\mu_0}{\beta}\left[\frac{J_n'(u)}{uJ_n(u)}+\frac{I_n'(w)}{wI_n(w)}\right]I_n(w)\sum_{m=0}^{\infty}\nu f_{nm}H_{m1} = 0,$$

$$n\left(\frac{1}{u^2}+\frac{1}{w^2}\right)\left[K_n(w)H_{n1}+I_n(w)\sum_{m=0}^{\infty}\nu f_{nm}H_{m1}\right]-\frac{\omega\epsilon_0}{\beta}\left[\frac{n_1^2J_n'(u)}{uJ_n(u)}+\frac{n_0^2K_n'(w)}{wK_n(w)}\right]K_n(w)G_{n1}$$
$$-\frac{\omega\epsilon_0}{\beta}\left[\frac{n_1^2J_n'(u)}{uJ_n(u)}+\frac{n_0^2I_n'(w)}{wI_n(w)}\right]I_n(w)\sum_{m=0}^{\infty}\nu g_{nm}G_{m1}=0. \quad (A.15)$$

ORCID iDs

Fam Le Kien https://orcid.org/0000-0002-3463-6053
Síle Nic Chormaic https://orcid.org/0000-0003-4276-2014

References

[1] Snyder A W and Love J D 1983 *Optical Waveguide Theory* (London: Chapman and Hall)
[2] Marcuse D 1989 *Light Transmission Optics* (Malabar, FL: Krieger)
[3] Okamoto K 2006 *Fundamentals of Optical Waveguides* (Amsterdam: Elsevier)
[4] Tong L, Gattass R R, Ashcom J B, He S, Lou J, Shen M, Maxwell I and Mazur E 2003 *Nature* **426** 816
[5] Nieddu T, Gokhroo V and Chormaic S N 2016 *J. Opt.* **18** 053001
[6] Solano P, Grover J A, Hoffman J E, Ravets S, Fatemi F K, Orozco L A and Rolston S L 2017 *Adv. At. Mol. Opt. Phys.* **66** 439
[7] Nayak K P, Sadgrove M, Yalla R, Kien F L and Hakuta K 2018 *J. Opt.* **20** 073001
[8] Balykin V I, Hakuta K, Kien F L, Liang J Q and Morinaga M 2004 *Phys. Rev.* A **70** 011401(R)
[9] Kien F L, Balykin V I and Hakuta K 2004 *Phys. Rev.* A **70** 063403
[10] Vetsch E, Reitz D, Sagué G, Schmidt R, Dawkins S T and Rauschenbeutel A 2010 *Phys. Rev. Lett.* **104** 203603
[11] Goban A, Choi K S, Alton D J, Ding D, Lacroûte C, Pototschnig M, Thiele T, Stern N P and Kimble H J 2012 *Phys. Rev. Lett.* **109** 033603
[12] Kien F L, Dutta Gupta S, Balykin V I and Hakuta K 2005 *Phys. Rev.* A **72** 032509
[13] Nayak K P, Melentiev P N, Morinaga M, Kien F L, Balykin V I and Hakuta K 2007 *Opt. Express* **15** 5431
[14] Nayak K P and Hakuta K 2008 *New J. Phys.* **10** 053003
[15] Kien F L, Balykin V I and Hakuta K 2006 *Phys. Rev.* A **73** 013819
[16] Sague G, Vetsch E, Alt W, Meschede D and Rauschenbeutel A 2007 *Phys. Rev. Lett.* **99** 163602
[17] Rajasree K S, Ray T, Karlsson K, Everett J L and Nic Chormaic S 2020 *Phys. Rev. Res.* **2** 012038
[18] Kien F L, Ray T, Nieddu T, Busch T and Nic Chormaic S 2018 *Phys. Rev.* A **97** 013821
[19] Ray T, Gupta R K, Gokhroo V, Everett J L, Nieddu T, Rajasree K S and Chormaic S N 2020 *New J. Phys.* **22** 062001
[20] Daly M, Truong V G, Phelan C F, Deasy K and Nic Chormaic S 2014 *New J. Phys.* **16** 053052
[21] Ding C, Loo V, Pigeon S, Gautier R, Joos M, Wu E, Giacobino E, Bramati A and Glorieux Q 2019 *New J. Phys.* **21** 073060
[22] Kien F L, Ruks L, Nic Chormaic S and Busch T 2020 *New J. Phys.* **22** 123007
[23] Wijngaard W 1973 *J. Opt. Soc. Am.* **63** 944
[24] Yamashita E, Ozeki S and Atsuki K 1985 *J. Lightwave Technol.* **3** 341
[25] Kishi N, Yamashita E and Kawabata H 1989 *J. Lightwave Technol.* **7** 902
[26] Huang H S and Chang H C 1990 *J. Lightwave Technol.* **8** 945
[27] Chang C S and Chang H C 1997 *J. Lightwave Technol.* **15** 1213
[28] Huang H S and Chang H-C 1989 *Opt. Lett.* **14** 90
[29] Chang C S and Chang H C 1997 *J. Lightwave Technol.* **15** 1225
[30] Povinelli M L, Lončar M, Ibanescu M, Smythe E J, Johnson S G, Capasso F and Joannopoulos J D 2005 *Opt. Lett.* **30** 3042
[31] Wang Z, Xie S, Jiang X, Babic F, Huang J, Pennetta R, Koehler J R and Russell P S J 2019 *ACS Photonics* **6** 2942
[32] Tong L, Hu L, Zhang J, Qiu J, Yang Q, Lou J, Shen Y, He J and Ye Z 2006 *Opt. Express* **14** 82
[33] Lodahl P, Mahmoodian S, Stobbe S, Rauschenbeutel A, Schneeweiss P, Volz J, Pichler H and Zoller P 2017 *Nature* **541** 473
[34] Chu S 1998 *Rev. Mod. Phys.* **70** 685
[35] Cohen-Tannoudji C N 1998 *Rev. Mod. Phys.* **70** 707
[36] Phillips W D 1998 *Rev. Mod. Phys.* **70** 721
[37] Dutta S K, Guest J R, Feldbaum D, Walz-Flannigan A and Raithel G 2000 *Phys. Rev. Lett.* **85** 5551
[38] Barredo D, Lienhard V, Scholl P, de Léséleuc S, Boulier T, Browaeys A and Lahaye T 2020 *Phys. Rev. Lett.* **124** 023201
[39] Malitson I H 1965 *J. Opt. Soc. Am.* **55** 1205
[40] Ghosh G 1997 *Handbook of Thermo-Optic Coefficients of Optical Materials with Applications* (New York: Academic)
[41] Birks T A, Wadsworth W J and Russell P S J 2000 *Opt. Lett.* **25** 1415
[42] Hammer J, Cavanna A, Pennetta R, Chekhova M V, Russell P S J and Joly N Y 2018 *Opt. Lett.* **43** 2320
[43] Scully M O and Zubairy M S 1997 *Quantum Optics* (Cambridge: Cambridge University Press)
[44] Abramowitz M and Stegun I A 2013 *Handbook of Mathematical Functions* (New York: Dover)